Magnetic Properties of Manganese Ferrite (MnFe$_2$O$_4$) Nanoparticles Synthesized by Co-Precipitation Method

Evrim Umut ⓘ
Dokuz Eylul University, School of Healthcare, Department of Medical Imaging Techniques, Balcova, Izmir, Turkey

ABSTRACT

In the presented study, manganese ferrite (MnFe$_2$O$_4$) nanoparticles were synthesized by applying a modified co-precipitation method based on the decomposition of metallic precursors in a liquid phase environment in the presence of surfactant oleic acid. The synthesized sample was then characterized with X-ray Diffraction (XRD), standard and high resolution Transmission Electron Microscopy (TEM) and Fourier Transform Infrared Spectroscopy (FTIR), which revealed that the as-prepared MnFe$_2$O$_4$ particles are monodispersed nanocrystals with an average size of 4.7 nm and well surrounded with dimeric oleic acid coating. The magnetic properties of nanoparticles were first investigated by means of Superconducting Quantum Interference Device (SQUID) magnetometry. The temperature and field dependent magnetization measurements showed that the MnFe$_2$O$_4$ nanoparticles exhibit superparamagnetic property with zero coercivity at room temperature and thermal irreversibility. The superparamagnetic behavior of MnFe$_2$O$_4$ nanoparticles was further confirmed by conducting zero field Mössbauer Spectroscopy measurements on nanoparticle powders. As to fulfill all the requirements like crystallinity, small size and superparamagnetism, the prepared oleic acid coated MnFe$_2$O$_4$ nanoparticles has the potential to be used in biomedical applications like targeted drug delivery, MRI and hyperthermia.

Keywords:
Superparamagnetism, Manganese ferrite, Magnetic nanoparticles, SQUID magnetometry, Mössbauer spectroscopy.

INTRODUCTION

Nanostructured transition metal oxides, also known as spinel ferrites, are commonly studied due to their potential use in a variety of biomedical applications such as magnetic resonance imaging, hyperthermia and targeted drug delivery [1]. The general formula for ferrite family is given as MFe$_2$O$_4$; M=Zn, Ni, Co, Mn, where depending on the Curie temperature, magnetic anisotropy and magnetic moment of the substitution metal M, the overall magnetic properties of ferrites can be adjusted in order to optimize their performance in these biomedical applications. In this manner, manganese ferrite MnFe$_2$O$_4$ is a good candidate with its relatively high magnetization and biocompatibility [2,3]. For these reasons, nanosized MnFe$_2$O$_4$ particles were deeply investigated in literature, where particles were synthesized with different techniques and their surfaces were functionalized with different capping agents.

In the beginning of 2000s, Z. J. Zhang and coworkers, in a series of papers, showed the effect of particle size and interparticle interactions on the general magnetic behavior of MnFe$_2$O$_4$ nanoparticles synthesized with reverse microemulsion method [4-7]. By grafting a wide variety of ligands on the surface of MnFe$_2$O$_4$ nanoparticles, they also studied the relationship between surface coordination chemistry and the magnetic properties [8]. In 2009, A. Yang et al. demonstrated the change in Neel temperature depending on the cation distribution in MnFe$_2$O$_4$ particles prepared with co-precipitation method [9]. Later Aslibeiki and his colleagues, reported observation of a superspin glass-like behavior in nanosized MnFe$_2$O$_4$ particles produced by ball-milling technique, where they attribute the origin of this behavior to dipolar interactions among particles [10]. Following these studies, first papers reporting the implementation of MnFe$_2$O$_4$ nanoparticles into biomedical applications were published: Tromsdorf et al. [11]

presented the proton NMR relaxivities of superparamagnetic $MnFe_2O_4$ suspensions in water as a measure of their MRI contrast enhancement efficiencies for the first time. H. Yang et al. published a more comprehensive research, where they investigated the cytotoxity and cellular uptake of such nanoparticles and compared their performance as MRI contrast agents by means of direct MR images both in-vitro and in-vivo [3]. Regarding the heat generation abilities of these particles D. H. Kim et al. focused on water dispersible surface modified MnFe2O4 nanoparticles, which are further coated with chitosan and can be loaded with drugs for possible drug delivery application. By obtaining infrared images of nanoparticle suspensions irradiated by a RF field, they revealed that these suspensions can be used as potential hyperthermia mediators [2].

In this study, we report the characterization results of oleic acid coated $MnFe_2O_4$ nanoparticles prepared with co-precipitation method and discuss the observed magnetic behavior of these particles on the basis of their physicochemical properties. The paper is organized as follows: In Section 2 the sample preparation procedure and the experimental details are briefly explained. The structural, surface and magnetic characterization results of properties of as-prepared $MnFe_2O_4$ nanoparticles are discussed in Section 3 and the concluding remarks are given in Section 4.

MATERIALS AND METHODS

$MnFe_2O_4$ nanoparticles were synthesized and in-situ coated with oleic acid (OA) following a modified chemical co-precipitation technique [12]. Briefly, a solution of 10 mmol $FeCl_3 \cdot 6H_2O$ and 5 mmol $MnCl_2 \cdot 6H_2O$ in 175 ml diethylene glycol (DEG) were mixed in a three neck flask for 1 h under magnetic stirring. By adding another separate 0.5 M NaOH solution in DEG and 4 hours of mixing under nitrogen (N_2) flow, the yellow color of the solution was gradually changed into brown. After heating the resulting solution to 210 °C of temperature, a mixture of oleic acid in DEG (8 mmol / 55 ml) was added. Finally, after 2 h, the solution was cooled down to room temperature and the particles were obtained as precipitate. After washing the precipitate with methanol and dispersing in toluene, as a size selection process, relatively larger particles were isolated from sample by subsequent precipitation, redispersing and centrifugation. All the chemical products were purchased from Sigma-Aldrich and Alfa Aeser company and used without further modification.

The structural characterization of synthesized particles were done by collecting XRPD (x-ray powder diffraction) patterns of the $MnFe_2O_4$ nanoparticles using a Rigaku D/Max-Ultima diffractometer working with Cu-K_α radiation produced under 40 kV and 40 mA, while the morphology

of the particles were investigated through standard and high resolution Transmission Electron Microscopy (TEM / HRTEM) images obtained with a JEOL JEM-2100F in bright field mode running with 200kV of acceleration voltage. The surface characterization of OA coated $MnFe_2O_4$ particles were realized by recording the infrared spectra with a Thermo Scientific ATR Fourier Transform Infrared (FTIR) spectrometer for wavenumbers between 4000-650 cm^{-1}.

The magnetic properties of as-prepared $MnFe_2O_4$ nanoparticles were investigated by conducting magnetometry experiments using a Quantum Design SQUID (Superconductiong-Quantum-Interference-Device) MPMS magnetometer. Magnetic field and temperature dependent magnetization measurements were performed on nanoparticle powders. Field dependent measurements were performed by changing the applied magnetic field between ± 5 T at room and at 5 K temperature, while the temperature dependent measurements were done in zero field cooling (ZFC) and field cooling (FC) mode. In ZFC mode first, the sample was cooled down to 5 K without any magnetic field and then the magnetization was measured by applying 100 Oe of constant field and heating the sample back to room temperature. In FC mode, the magnetization is measured under the same static field by cooling down the sample back to 5 K temperature.

The room temperature [57]Fe Mössbauer spectra of powder nanoparticle sample was obtained by using a spectrometer equipped with a [57]Co γ-radiation source in rhodium matrix. The measurements were done in the transmission geometry in constant acceleration mode with a triangular shape of varying Doppler velocity, where the velocity calibration was done using a 10-μm thick Fe foil and the isomer chemical shifts were determined with respect to Fe.

RESULTS AND DISCUSSION

Fig.1 shows the X-ray powder diffraction (XRPD) pattern of as-prepared $MnFe_2O_4$ nanoparticles confirming the crystal nature of nanoparticles with cubic spinel structure. The peaks are broadened as compared to bulk crystals due to the nanoscale and the size of the nanocrystals can be calculated according to Debye-Scherrer formalism (Eq.1). In Eq.1, λ is the wavelength of used Cu-K_α radiation, θ is the half angle (in radians) at which the broadened Bragg reflection observed and β is the FWHM (full width at half maximum intensity) of the broadened peak.

$$D = \frac{0.9\lambda}{\beta\cos\theta} \tag{1}$$

By applying this formalism to (311) reflection peak, which is the least effected from experimental line broadening contributions, a mean crystallite size of d= 4.5 nm was calculated. This information was further validated with
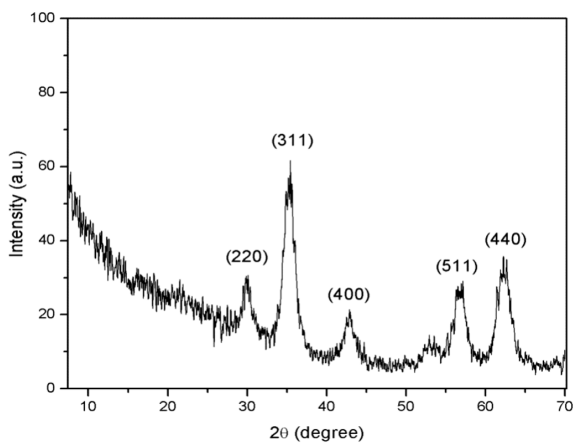
Figure 1. XRPD pattern of $MnFe_2O_4$ nanoparticles with indexing of peaks according to cubic spinel structure

Figure 3. Infrared transmission spectra of oleic acid (OA) coated $MnFe_2O_4$ nanoparticle powder

TEM-HRTEM images of nanoparticles shown in Fig. 2a. The images show that the synthesized particles are monodispersed with almost spherical shape and separated from each other due to OA coating, however some agglomerates are present together with isolated particles. The size distribution histogram graph deduced from TEM images is also given in Fig. 2b, which is fitted with log-normal distribution function (solid red line) given in Eq.2 with a mean value of d_{mean}=4.77 nm and standard deviation of σ =0.3 nm, as consistent with XRPD results.

$$f(d) = \frac{1}{d\sqrt{2\pi\sigma^2}} exp\left[\frac{-ln\left(\frac{d}{d_{mean}}\right)^2}{2\sigma^2} \right] \quad (2)$$

Surface characterization of oleic acid (OA) coated $MnFe_2O_4$ nanoparticles were done by recording FTIR spectra as shown in Fig.3. The set of peaks observed in 3500-4000 cm^{-1} range are fingerprints of the vibrations of the hydroxyl group (O-H) in OA. One can associate the double peak lo-

cated around 2350 cm^{-1} with C-H stretching (asymmetric and symmetric mode) in the long ethyl chain (CH_2) in OA and methyl group (CH_3) at the end of this chain. Moreover, the strong peak at 1745 cm^{-1} can be attributed to C=O stretching, while the bands at 1512 cm^{-1}, 1370 cm^{-1} and 1210 cm^{-1} can be due to the C-O elongation and angular deformation of C-O-H bonds, which implies that OA molecules were successfully coated around the $MnFe_2O_4$ surface. One should here also state that; a broad characteristic peak for the intrinsic metal-oxygen bond vibrations occurring in the tetrahedral sites of the spinel structured $MnFe_2O_4$ magnetic core is generally observed around 600-570 cm^{-1} [3,13], which is unfortunately out of the scanning range of the used spectrometer in this study. However, the tail of this peak can be hardly seen at the shortest wavenumber limit of 650 cm^{-1} in Fig.3.

The magnetic behavior of as-prepared $MnFe_2O_4$ nanoparticles was investigated by means of magnetometry measurements. Fig.4 shows temperature (M-T) and field dependent (M-H) magnetization curves collected on powders.
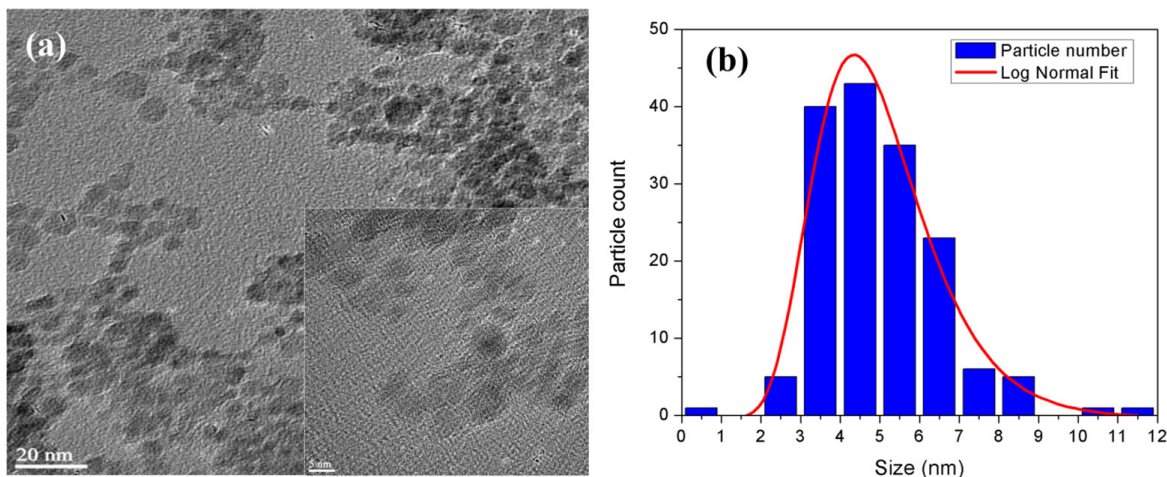
Figure 2. TEM (a) and HRTEM (inset of Fig. 2a) images of OA coated $MnFe_2O_4$ nanoparticles and size distribution histogram (b). Red curve shows fit with log-normal distribution function (Eq.2)

The zero coercivity observed at room temperature M-H curve (Fig.4a), together with the thermal irreversibility i.e. splitting of zero field cooling - field cooling (ZFC-FC) curves in M-T measurements (Fig.4b) indicates that the nanoparticles possess superparamagnetic behavior with thermally activated magnetization reversal and blocking phenomena. In M-H curve it is observed that the sample reaches a saturation magnetization of 55 emu/g. This value is smaller than the reported magnetization for bulk $MnFe_2O_4$ (82 emu/g) and the discrepancy originates from the enhanced surface-to-volume ratio of nanoparticles, where the canted surface spins do not contribute to overall magnetization. On the other hand, in M-T curve (Fig.4b) the average blocking temperature, which can be assigned as the maxima of ZFC curve, is approximately T_B=40 K and assuming that the particles' magnetic moments obey Arrhenius like reversal (Eq.3), as a first approximation one can roughly estimate a total magnetic anisotropy energy K_{total}=2.8x10^4 J/m^3 calculated by using the blocking condition $T_B \cong K_{total} V/21k_B$ obtained for τ = 1 s at T=T_B and τ_0=10^{-9} s ,where k_B is the Boltzmann constant and V is the particle volume [14].

$$\tau = \tau_0 \exp\left(\frac{K_{total}V}{k_B T}\right) \quad (3)$$

However, another observation on Fig.4b is that in FC curve the magnetization more or less stays constant below the blocking temperature (T<T_B) instead of increasing with the same rate as at high temperatures (T>T_B), which is an indication that interparticle interactions are effective and give rise to collective motion of particle moments i.e. spin-glass like behavior [15]. In this case, particle moment relaxation can be better described by Vogel-Fulcher-Tammann [16-18] like formalism (Eq.4) rather than the Arrhenius law and one should take into account that the above calculation for total magnetic anisotropy energy K_{total} is not very precise since it takes significant contribution from interactions among particles.

$$\tau = \tau_0 \exp\left(\frac{K_{total}V}{k_B\left(T - T_0\right)}\right) \quad (4)$$

It is also worthwhile to mention about the evolution of some anisotropy dependent parameters i.e. coercivity (coercive field) H_C, saturation magnetization M_S and remanent magnetization M_r with respect to the temperature. For single-domain particles, in the range of T<T_B the temperature dependence of coercivity H_C follows the so called Kneller's law [19,20]:

$$H_c(T) = H_c(0)\left[1 - \left(\frac{T}{T_B}\right)^{1/2}\right] \quad (5)$$

where T_B is the blocking temperature and $H_c(0)$ is the coercivity value at T=0K, which is equal to $H_c(0)$=2K_{total} / $\mu_0 M_S$ (in S.I. units) with μ_0 and M_s being the permeability of vacuum and the saturation magnetizationg at zero temperature, respectively. In Eq.5, by substituting the value of H_C=240 Oe for T=5K obtained from M-H curve and the value of T_B=40 K obtained from M-T curve given in Fig.4, one calculates $H_C(0)$=370 Oe and the expected behavior of $H_c(T)$ can be depicted as in Fig.5a. The remanent magnetization M_r should follow the same trend with coercivity as to reach zero remanence for T ≥ T_B due to the fact that the thermal energy overcomes anisotropy energy barrier giving rise to superparamagnetic regime [19,21]. On the other side, the temperature dependence of M_S below the Curie temperature is generally described by Bloch's law [22] (owing to the behavior of spin wave excitations, particularly "magnons") as $M_S(T)$=$M_S(0)$[1-(T/T_0)$^\alpha$], where the exponent is α =3/2 for bulk systems and α <2 for nanosized materials [23,24]. Fig.5b shows a simulated curve of $M_S(T)$ (for $M_S(0)$=73emu/g, T_0=650K, α =1.55) as to contain the experimental M_S values obtained from M-H curves at 300K and 5K given in Fig.4a. One should here note that, a more general approach descri-
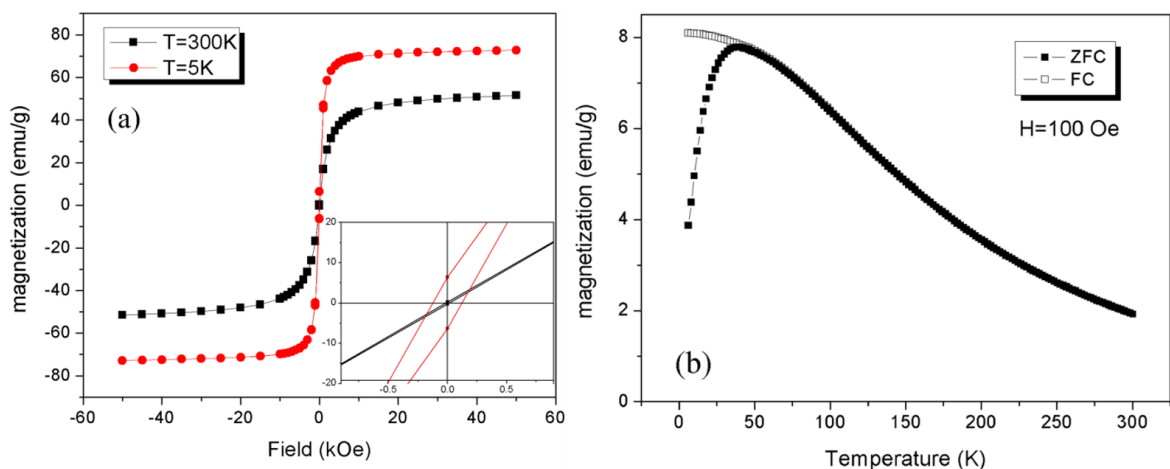
Figure 4. Magnetization curves as a function of magnetic field (a) and temperature (b) obtained on MnFe$_2$O$_4$ nanoparticles in powder. Inset graph in (a) shows the magnetization data in enlarged scale
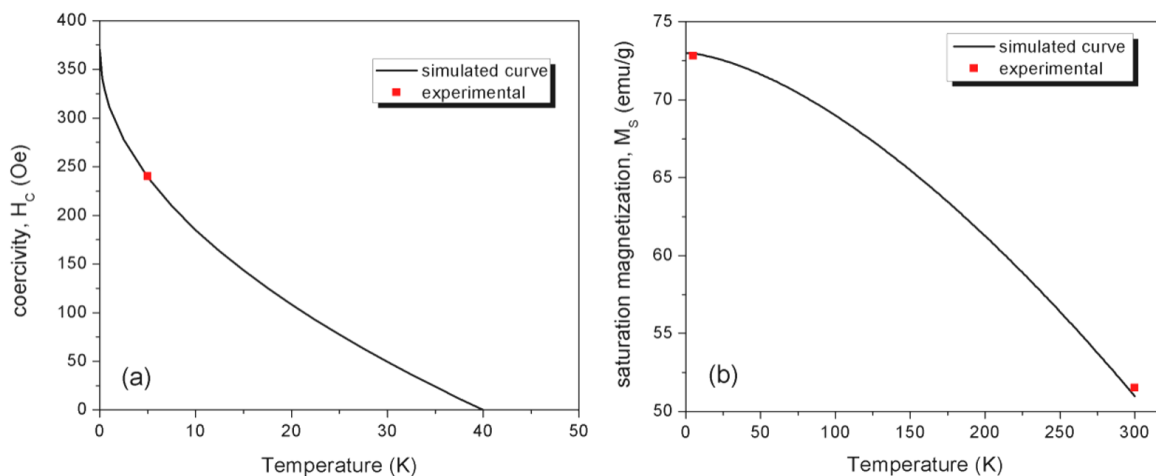
Figure 5. Simulated curves of (a) coercivity H_C according to Kneller's law for $H_C(0)$=370 Oe, T_B=40 K and (b) saturation magnetization M_S using Bloch's law for $M_S(0)$=73emu/g, T_0=650K, α =1.55.

bing the temperature dependence of M_S takes into account the so called "surface spin freezing" effect manifesting itself at very low temperatures. In this case, the M_S is given by modified Bloch's law in the form $M_S(T)=M_S(0)[(1-(T/T_0)^{\alpha} +A_0\exp(-T/T_f)]$, where the additional second term represents surface contribution with T_f being the freezing temperature at which the surface spins of nanoparticle become frozen (quenched) in a spin-glass like structure [24].

The magnetic properties of OA coated $MnFe_2O_4$ particles were further characterized with zero field ^{57}Fe Mössbauer spectroscopy. The technique measures the transitions between nuclear ground state (I_g=1/2) and excited state (I_e=3/2) of iron, which are splitted due to the quadrupolar interactions and/or hyperfine (Zeeman) interactions hence acts as a local probe providing information about the charge distribution, oxidation state and symmetry. The room temperature Mössbauer spectra of $MnFe_2O_4$ nanoparticles is shown in Fig.6. The observed intense absorption line at the centre (an asymmetric doublet) is a signature for superparamagnetic behavior of these nanoparticles, where the hyperfine field B_{hf} sensed by ^{57}Fe nuclei fluctuates much faster than the Larmor frequency of nuclear moments. In particular, at room temperature during one Larmor precession time thermal excitation is high enough to reorient the electronic spins more than several times to cancel the average value of B_{hf}, which causes the observation of magnetically split levels (sextet) in Mössbauer spectra [25]. This is consistent with results obtained by magnetometry measurements, however considering that the Mössbauer experiment has a characteristic time scale (approximately 10^{-8} s) much shorter than the magnetometry technique (typically in the range of 1-100 seconds), a magnetic system appears superparamagnetic in magnetometry experiment may not appear superparamagnetic in Mössbauer spectroscopy, but observation of blocking features for such small nanoparticles (~4.5 nm for our
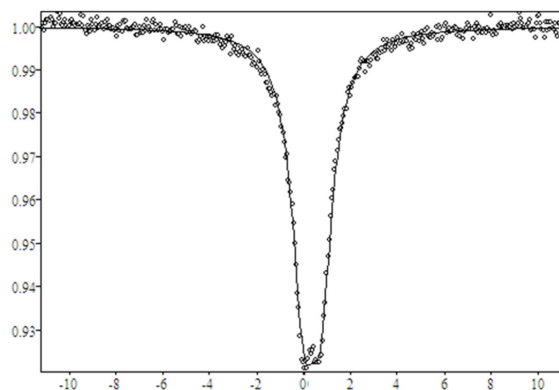
Figure 6. Room temperature ^{57}Fe Mössbauer spectra of $MnFe_2O_4$ nanoparticles (hollow circles) and theoretical fit (solid line)

$MnFe_2O_4$ particles) is only possible at low temperatures and/or under high magnetic fields.

On the other hand, the observation of a doublet (instead of a singlet line) is unambiguously is a result of quadrupolar splitting due to the coupling of Fe with Mn, which has a nuclear spin of I=5/2. In particular, the electric field gradient (EFG) induced by the quadrupolar Mn nuclei gives rise to a splitting of the excited state levels (I=3/2) of Fe nucleus and the line separation of the doublet gives the energy difference of these splitted levels. Mössbauer spectra was fitted with a special program using a least square technique (Fig.6) [26]. Table 1 summarizes the fit parameters, where A and Γ are the intensity and width of doublet lines, respectively, IS is the isomer chemical shift and QS is quadrupolar splitting in velocity unit (mm/s).

Table 1. The output parameters for fit shown in Fig.6. A: line intensity, Γ : line width, IS: isomer chemical shift, QS: quadrupolar splitting

A_1 (imp.)	A_2 (imp.)	A_1/A_2	Γ_1 (mm/s)	Γ_2 (mm/s)	IS (mm/s)	QS (mm/s)
-35898± 717	-34656± 717	1.036± 0.041	1.223± 0.014	1.223± 0.002	0.337± 0.008	0.734± 0.009

CONCLUSION

As a promising alternative to most widely used iron oxides in biomedical applications, $MnFe_2O_4$ particles were synthesized and in situ coated with organic surfactant by following a modified co-precipitation method. The structural characterization by means of XRD, TEM and surface characterization with FTIR experiments revealed that the as-prepared $MnFe_2O_4$ particles are monodispersed nanocrystallites with an average particle size around 4.5 nm and successfully coated with oleic acid. The SQUID magnetometry measurements performed on powder showed that the $MnFe_2O_4$ particles exhibit superparamagnetic behavior with zero coercivity at room temperature and thermal irreversibility in zero field cooled - field cooled (ZFC-FC) curves. From ZFC-FC curves the mean blocking temperature was found to be around T_B=40 K and the total magnetic anisotropy energy was approximately calculated as K_{total}=2.8x10^4 J/m^3. The observed room temperature saturation magnetization M_S=55 emu/g, resulted to be smaller than the value of bulk $MnFe_2O_4$ due to the disordered surface spins and the non-increasing behavior of magnetization below T_B in FC curve implied spin-glass like collective particle moment reversal due to interparticle interactions. Based on the deduced parameters from experimental M-H and M-T curves, the expected temperature dependence of coercivity H_c(T) and saturation magnetization M_s(T) were simulated using Kneller's and Bloch's law, respectively. Room temperature ^{57}Fe Mössbauer spectroscopy measurements further confirmed the superparamagnetic property and the existence of Mn in the structure of $MnFe_2O_4$ based on the quadrupolar splitting in the spectral line. By fitting the Mössbauer spectra the magnitude of the quadrupolar splitting and isomer chemical shift were obtained. As a future study, in order to obtain the cation distribution in crystallite sites of $MnFe_2O_4$ and calculate the individual magnetic moment values further Mössbauer measurements at low temperatures are planned.

ACKNOWLEDGEMENTS

References

1. Umut E, Surface modification of nanoparticles used in biomedical applications, in: Mahmood Aliofkhazraei (Ed.), Modern Surface Engineering Treatments, IntechOpen Ltd., London, pp.185–208, 2013.

2. Kim DH, Nikles DE, Brazel CS. Synthesis and characterization of multifunctional chitosan – MnFe2O4 nanoparticles for magnetic hyperthermia and drug delivery. Materials 3 (2010) 4051–4065.

3. Yang H, Zhang C, Shi X, Hu H, Du X, Fang Y, Ma Y, Wu H, Yang S. Water–soluble superparamagnetic manganese ferrite nanoparticles for magnetic resonance imaging. Biomaterials 31 (2010) 3667–3673.

4. Liu C, Zou B, Rondinone AJ, Zhang ZJ. Reverse micelle synthesis and characterization of superparamagnetic MnFe2O4 spinel ferrite nanocrystallites. Journal of Physical Chemistry B 104 (2000) 1141–1145.

5. Liu C, Zhang ZJ. Size–dependent superparamagnetic properties of Mn spinel ferrite nanoparticles synthesized from reverse micelles. Chemistry of Materials 13 (2001) 2092–2096.

6. Rondinone AJ, Liu C, Zhang ZJ, Determination of magnetic anisotropy distribution and anisotropy constant of manganese spinel ferrite nanoparticles. Journal of Physical Chemistry B 105 (2001) 7967–7971.

7. Vestal CR, Song Q, Zhang ZJ. Effects of interparticle interactions upon the magnetic properties of CoFe2O4 and MnFe2O4 nanocrystals. Journal of Physical Chemistry B 108 (2004) 18222–18227.

8. Vestal CR, Zhang ZJ. Effects of surface coordination chemistry on the magnetic properties of MnFe2O4 spinel ferrite nanoparticles. Journal of American Chemical Society 125 (2003) 9828–9833.

9. Yang A, Chinnasamy CN, Greneche JM, Chen Y, Yoon SD, Chen Z, Hsu K, Cai Z, Ziemer K, Vittoria C, Harris VG. Enhanced Neel temperature in Mn ferrite nanoparticles linked to growth–rate–induced cation inversion. Nanotechnology 20 (2009) 185704–185713.

10. Aslibeiki B, Kameli P, Salamati H, Eshraghi M, Tahmasebi, T. Superspin glass state in MnFe2O4 nanoparticles. Journal of Magnetism and Magnetic Materials 322 (2010) 2929–2934.

11. Tromsdorf UI, Bigall NC, Kaul MG, Bruns OT, Nikolic MS, Mollwitz B, Sperling RA, Reimer R, Hohenberg H, Parak WJ, Förster S, Beisiegel U, Adam G, Weller H. Size and surface effects on the MRI relaxivity of manganese ferrite nanoparticle contrast agents. Nano Letters 7 (2007) 2422–2427.

12. Caruntu D, Remond Y, Chou NH, Jun MJ, Caruntu G, He J, Goloverda G, O'Connor C, Kolesnichenko V. Reactivity of 3D transition metal cations in diethylene glycol solutions: Synthesis of transition metal ferrites with the structure of discrete nanoparticles complexed with longchain carboxylate anions. Inorganic Chemistry 41 (2002) 6137-6146.

13. Hosseini SH, Mohseni SH, Asadnia A, Kerdari H. Synthesis and microwave absorbing properties of polyaniline / MnFe2O4 nanocomposite. Journal of Alloys and Compounds 509 (2011) 4682-4687.

14. Umut E, Coşkun M, Pineider F, Berti D, Güngüneş H. Nickel ferrite nanoparticles for simultaneous use in magnetic resonance imaging and magnetic fluid hyperthermia,

Journal of Colloid and Interface Science 5520 (2019) 199–209.

15. Dormann JL, Bessais L, Fiorani D. A dynamic study of small interacting particles: superparamagnetic model and spin–glass laws. Journal of Physics C 21 (1988) 2015–2034.

16. Vogel H. The law of relation between the viscosity of liquids and the temperature. Physikalische Zeitschrift 22 (1921) 645–646.

17. Fulcher GS. Analysis of recent measurements of viscosity of glasses. Journal of American Ceramics Society 8 (1925) 339–355.

18. Tammann G, Hesse W. The dependence of viscosity upon the temperature of supercooled liquids. Zeitschrift für Anorganische und Allgemeine Chemie 156 (1926) 245–257.

19. Kneller EF, Luborsky FE. Particle size dependence of coercivity and remanence of single–domain particles. Journal of Applied Physics 34 (1963) 656–658.

20. Osman NSE, Moyo T. Temperature dependence of coercivity and magnetization of Sr1/3Mn1/3Co1/3Fe2O4 ferrite nanoparticles. Journal of Superconductivity and Novel Magnetism 29 (2016) 361-366.

21. Chatterjee BK, Ghosh CK, Chattopadhyay KK. Temperature dependence of magnetization and anisotropy in uniaxial NiFe2O4 nanomagnets: Deviation from the Callen–Callen power law. Journal of Applied Physics 116 (2014) 153904.

22. Kaplan H. A spin–wave treatment of the saturation magnetization of ferrites. Physical Review 86 (1952) 121.

23. Masina P, Moyo T, Abdallah HMI. Synthesis, structure and magnetic properties of ZnxMg1–xFe2O4 nanoferrites. Journal of Magnetism and Magnetic Matterials 381 (2015) 41.

24. Gao RR, Zhang Y, Yu W, Xiong R, Shi J. Superparamagnetism and spin–glass like state for the MnFe2O4 nano–particles synthesized by the thermal decomposition method. Journal of Magnetism and Magnetic Matterials 324 (2012) 2534–2538.

25. Yoshida Y, Langouche G. (Eds.) Mössbauer Spectroscopy. Springer, 2013.

26. Semenov VG, Panchuk VV. Mössbauer Spectra Processing Program MossFit (private communication)